

THE OFFICIAL MAGAZINE OF THE OCEANOGRAPHY SOCIETY

Oceanography

CITATION

Farrar, J.T., L. Rainville, A.J. Plueddemann, W.S. Kessler, C. Lee, B.A. Hodges, R.W. Schmitt, J.B. Edson, S.C. Riser, C.C. Eriksen, and D.M. Fratantoni. 2015. Salinity and temperature balances at the SPURS central mooring during fall and winter. *Oceanography* 28(1):56–65, <http://dx.doi.org/10.5670/oceanog.2015.06>.

DOI

<http://dx.doi.org/10.5670/oceanog.2015.06>

COPYRIGHT

This article has been published in *Oceanography*, Volume 28, Number 1, a quarterly journal of The Oceanography Society. Copyright 2015 by The Oceanography Society. All rights reserved.

USAGE

Permission is granted to copy this article for use in teaching and research. Republication, systematic reproduction, or collective redistribution of any portion of this article by photocopy machine, reposting, or other means is permitted only with the approval of The Oceanography Society. Send all correspondence to: info@tos.org or The Oceanography Society, PO Box 1931, Rockville, MD 20849-1931, USA.

Salinity and Temperature Balances

at the SPURS Central Mooring
During Fall and Winter

By J. Thomas Farrar, Luc Rainville,
Albert J. Plueddemann, William S. Kessler,
Craig Lee, Benjamin A. Hodges,
Raymond W. Schmitt, James B. Edson,
Stephen C. Riser, Charles C. Eriksen,
and David M. Fratantoni



ABSTRACT. One part of the Salinity Processes in the Upper-ocean Regional Study (SPURS) field campaign focused on understanding the physical processes affecting the evolution of upper-ocean salinity in the region of climatological maximum sea surface salinity in the subtropical North Atlantic (SPURS-1). An upper-ocean salinity budget provides a useful framework for increasing this understanding. The SPURS-1 program included a central heavily instrumented mooring for making accurate measurements of air-sea surface fluxes, as well as other moorings, Argo floats, and gliders that together formed a dense observational array. Data from this array are used to estimate terms in the upper-ocean salinity and heat budgets during the SPURS-1 campaign, with a focus on the first several months (October 2012 to February 2013) when the surface mixed layer was becoming deeper, fresher, and cooler. Specifically, we examine the salinity and temperature balances for an upper-ocean mixed layer, defined as the layer where the density is within 0.4 kg m^{-3} of its surface value. The gross features of the evolution of upper-ocean salinity and temperature during this fall/winter season are explained by a combination of evaporation and precipitation at the sea surface, horizontal transport of heat and salt by mixed-layer currents, and vertical entrainment of fresher, cooler fluid into the layer as it deepened. While all of these processes were important in the observed seasonal (fall) freshening at this location in the salinity-maximum region, the variability of salinity on monthly-to-intraseasonal time scales resulted primarily from horizontal advection.

INTRODUCTION

The initial (2012–2013) Salinity Processes in the Upper-ocean Regional Study (SPURS) field campaign in the North Atlantic (SPURS-1) and the upcoming SPURS-2 (anticipated for 2016–2017) field campaign in the Pacific are intended to improve understanding of the physical processes influencing upper-ocean salinity. Interest in understanding these processes is partly motivated by the finding that upper-ocean salinity is a sensitive indicator of changes in the global water cycle (e.g., Durack and Wijffels, 2010; Durack et al., 2012; Durack, 2015, in this issue), which is inextricably tied to evaporation and precipitation over the ocean (Schmitt, 2008). There has been a phenomenal improvement in our ability to measure salinity in the global ocean during the last 10 years, as the Argo float array and satellite salinity measurements from the Aquarius and the European Soil Moisture and Ocean Salinity (SMOS) satellites have become available. We need to better understand the physical processes influencing upper-ocean salinity in order to fully exploit these global

measurements. To that end, it is important to define the relative roles of air-sea fluxes and ocean dynamics in observed salinity changes, and to determine the nature of salinity variations that are not resolved by these coarse global measurements.

Regions of long-term sea surface salinity (SSS) extremes are of special interest for studying the links between salinity and the global water cycle because recent observations show that salty regions are becoming saltier and fresh regions fresher (e.g., Durack and Wijffels, 2010). The SPURS-1 field campaign took place over a one-year period during 2012–2013 in the North Atlantic Ocean subtropical gyre, near the location where SSS is highest on average (Figure 1a). The relatively salty waters found at the surface here are subducted and carried downward and southward in a “river of salt” by large-scale currents (Schmitt and Blair, 2015, in this issue) and eventually westward into the Gulf Stream and northward into the subpolar oceans (e.g., Qu et al., 2013). The overarching goal of the SPURS field campaign and associated modeling activities is to improve

understanding of the physical processes influencing the formation and evolution of the salinity maximum.

One particularly useful way to gain insight into the various physical processes that influence ocean salinity is to make a “salt budget.” The basic idea of a salt budget is to consider a given volume, or an imaginary “box,” within the ocean. Salinity inside the box can only change if salt is transported through one of the box’s six faces. (This transport of salt across an area is called a *salt flux*.) Of course, the ocean is a dynamic fluid, with many physical processes causing many kinds of motions (e.g., waves, currents, and eddies on scales of centimeters to thousands of kilometers), and salt is transported vertically and horizontally across all six faces of the box.

In this article, we use SPURS-1 measurements to examine one view of upper-ocean salinity and heat budgets, with a fairly limited focus on the “surface layer” and the first several months of SPURS-1, when the surface layer of the salinity maximum region of the North Atlantic was deepening, freshening, and cooling during fall and winter (October 2012 to February 2013).

CONSERVATION OF SALT AND HEAT: SALINITY AND TEMPERATURE BALANCES

A salt budget, as the name suggests, is a process of accounting for all of the salt entering or leaving a control volume (or box) in the ocean. This exercise does not directly tell us what particular physical phenomena are causing changes in salinity within the box, but it does help narrow our focus to particular physical processes that are influencing salinity. Salinity variations occur on a vast range of temporal and spatial scales, from minutes to decades (e.g., Riser et al., 2015, in this issue) and from centimeter to global scales. Varying the size and shape of our box and the temporal averaging that we

use to estimate the terms in the salt budget will emphasize different processes affecting salinity on different temporal and spatial scales.

The conservation of salt can be expressed mathematically as

$$\frac{\partial S}{\partial t} + \nabla \cdot \bar{u}S + \nabla \cdot \bar{F} = 0 \quad (1)$$

where S is the salinity, \bar{u} is the

three-dimensional velocity vector, F is the diffusive or turbulent salinity flux, and $\bar{u}S$ is the salinity flux due to ocean currents (e.g., Gill, 1982). This equation can be thought of as describing the change of salinity within the box—it states that the rate of change of salinity at a location ($\frac{\partial S}{\partial t}$) is due to differences in salt transport

by ocean currents ($\bar{u}S$) on the box's six faces (represented by the “ $\nabla \cdot$ ” divergence operator) or by differences in F on the six faces. It is convenient to integrate Equation 1 vertically over the ocean surface mixed layer, which has relatively small vertical gradients of salt (and other properties) due to the mixing action of winds and nighttime convection.

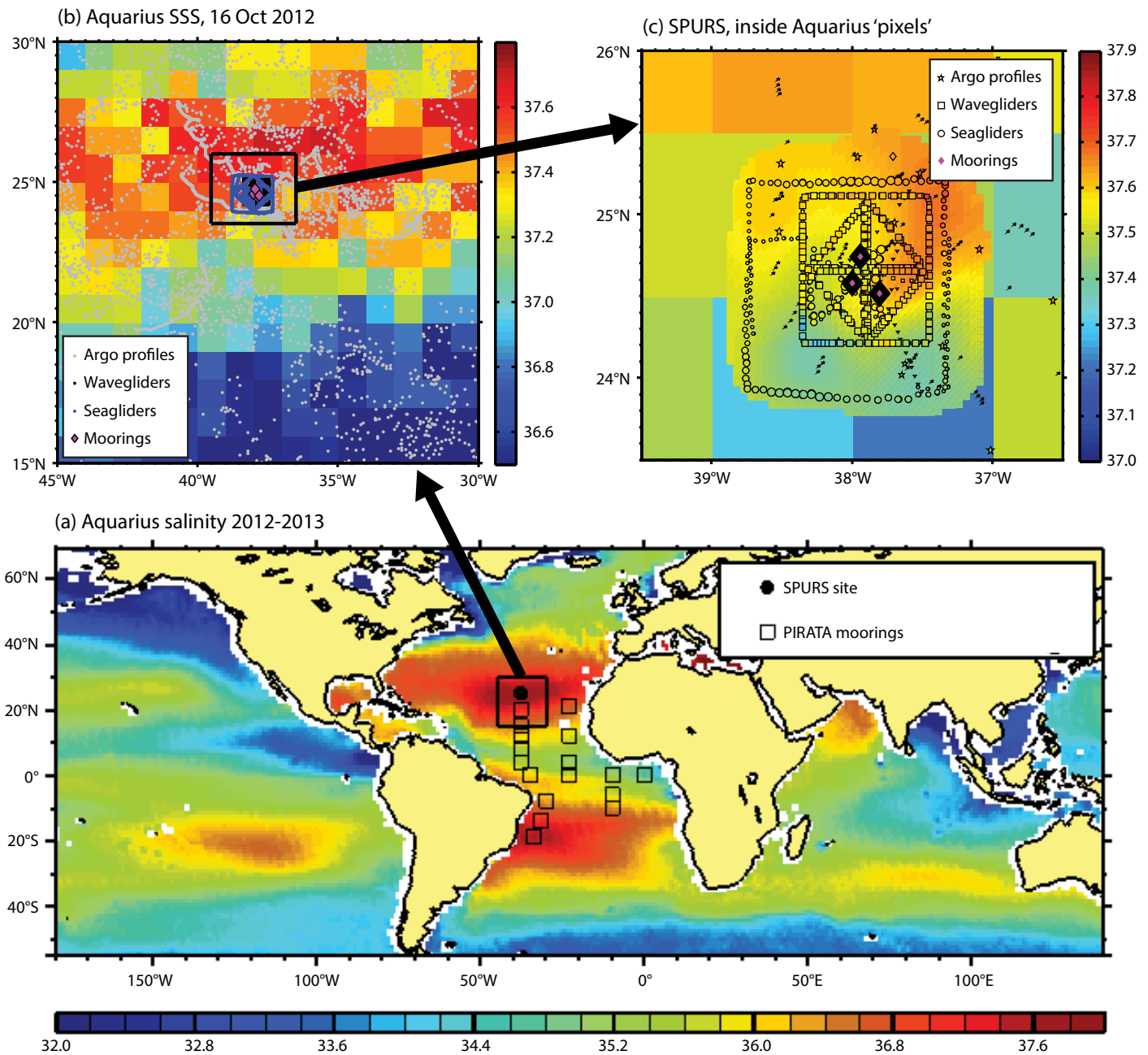


FIGURE 1. (a) Mean salinity over 2012–2013 from the Aquarius satellite (colored contours). The nominal location of the Salinity Processes in the Upper-ocean Regional Study (SPURS) field campaign in the subtropical Atlantic (SPURS-1) is indicated by a large black box. This broader SPURS study region is sometimes referred to as the “large SPURS box.” (b) A close-up view inside the large SPURS box, showing the surface salinity field during the first month of SPURS-1 from Aquarius and the distribution of some SPURS measurements within the study region. (c) A close-up view of the inner array of SPURS measurements showing the SPURS-1 measurement locations and the surface salinity field during October 2012. SPURS measurements allow a view of the salinity field on scales smaller than the ~100 km footprint of the Aquarius radiometer.

Performing this vertical integration from the sea surface to the base of the mixed layer, h , and noting that seawater is nearly incompressible ($\nabla \cdot \bar{\mathbf{u}} = 0$) leads to the following equation for the evolution of the layer-average salinity:

$$\frac{\partial \bar{S}}{\partial t} = -\bar{\mathbf{u}} \cdot \nabla \bar{S} + \frac{\hat{S}_{-h}}{h} \left(\frac{\partial h}{\partial t} \right) - \frac{F_{-h}}{h} + \frac{(E-P)S_o}{h} + R_s \quad (2a)$$

(Rate of change = advection + entrainment + turbulent flux + surface flux + residual)

$$R_s = -\bar{\mathbf{u}} \cdot \nabla \bar{S} - w \frac{\partial \bar{S}}{\partial z} \quad (2b)$$

where \bar{S} is defined as the layer-average salinity, $\bar{\mathbf{u}}$ is the layer-average horizontal velocity, quantities with hats (e.g., \hat{S}) indicate the vertically varying deviation from the average, the subscript $-h$ denotes the value at the base of the mixed layer, F_{-h} is the vertical turbulent salinity flux at depth h , E is the rate of evaporation from the sea surface, and P is the precipitation rate. The quantity R_s is a “residual” term containing terms that we will not evaluate explicitly here. Note that the lower boundary of the box (the base of the surface mixed layer) can change with time. The rate of change of mixed-layer salinity is a result of contributions from horizontal advection (i.e., currents carrying relatively salty water into the box), entrainment of fluid into the layer, turbulent exchange of fluid across the layer base, and surface fluxes (evaporation or precipitation). There are subtleties in the choice of definition of mixed-layer depth (h), but we define it here as the depth where the potential density increases by some prescribed value relative to its surface value.

Evaporation and precipitation at the sea surface do not actually change the amount of salt in the ocean, but they do dilute or concentrate the seawater and thus affect salinity. (Condensation on the sea surface can have the same effect as precipitation, but it is a much smaller contribution and is neglected here.)

Evaporation and precipitation represent freshwater fluxes and mass fluxes at the ocean surface. If we neglect the relatively small effects of evaporation and precipitation on the amount of water in our “box,” we can write evaporation and precipitation as a “virtual salt flux,” $(E-P)S_o$ (Gill, 1982; Beron-Vera et al., 1999), where S_o is the salinity at the surface.

The particular combination of terms on the right-hand side of Equation 2 is not unique, partly because the incompressibility of seawater links the horizontal and vertical velocity, and there are other ways of formulating the mixed-layer salinity balance equation (e.g., Foltz et al., 2004). While all of the terms in Equation 2, or alternative formulations of the integrated conservation equation, are mathematically well defined, the connection of the horizontal and vertical velocities and the different ways of grouping terms in the vertically averaged conservation equations leads to some ambiguity in interpreting particular terms as “vertical advection,” “horizontal advection,” or “entrainment” (also discussed by Cronin et al., 2013). This ambiguity is acceptable, keeping in mind that the ultimate goal of this budgeting exercise is to help us home in specifically on the physical processes that influence upper-ocean salinity.

There are equations for temperature that are analogous to the salt conservation equation and the mixed-layer salinity balance equation. We also examine the temperature balance for comparison with the salinity balance. The mixed-layer temperature balance is

$$\frac{\partial \bar{T}}{\partial t} = -\bar{\mathbf{u}} \cdot \nabla \bar{T} + \frac{\hat{T}_{-h}}{h} \left(\frac{\partial h}{\partial t} \right) - \frac{Q_{-h}}{\rho c_p h} + \frac{Q_o}{\rho c_p h} + R_T \quad (3)$$

where the terms are analogous to those in Equation 2: T is temperature, Q_o is the surface heat flux, Q_{-h} is the turbulent heat flux at the base of the mixed layer (depth h), c_p is the specific heat capacity, ρ is density, and R_T is the same as Equation 2b but with T replacing S .

THE SPURS OBSERVATIONAL ARRAY

The goal of quantifying the upper-ocean salinity budget motivated development of a “nested” observing strategy that would measure important physical processes at a range of temporal and spatial scales. Estimating the terms of the budget required characterizing salinity changes within an upper-ocean control volume, along with salt (freshwater) fluxes across the top (sea surface), bottom, and side boundaries. At the basin scale of the North Atlantic Ocean, we have an interesting and exciting new view of the ocean salinity field from the developing global ocean observing system, which includes the Aquarius/SAC-D and SMOS satellite missions, the global array of Argo floats, volunteer observing ships, and the multinational PIRATA (Prediction and Research Moored Array in the Tropical Atlantic) mooring array (Bourlès et al., 2008). The particular central location of the SPURS-1 campaign (around 25°N, 38°W) was chosen to tie in with and extend these larger, more sustained efforts (e.g., Figure 1a). At a somewhat smaller, regional scale of about 1,500 km, the SPURS-1 program enhanced the existing sustained observing system by working with the PIRATA program to augment measurements taken by the existing 20°N buoy, requesting increased sampling of the region by the National Oceanic and Atmospheric Administration (NOAA) Volunteer Observing Ship program, and deploying extra Argo floats and surface drifters in the region (e.g., Figure 1b).

On an even smaller scale, comparable to the Aquarius microwave antenna’s ~100 km footprint on the sea surface (the Aquarius “pixel scale”), the SPURS-1 measurement design included a dense array of moorings and gliders (Figure 1c and Figure 2). A heavily instrumented central mooring measured surface meteorology and vertical and temporal variations in water temperature, salinity, and velocity. Two nearby surface moorings provided time series of vertical profiles of temperature and salinity. With the

central mooring, these moorings formed a triangle that was about 20 km on a side. Three autonomous Wave Gliders sampled a 100 km square box centered on the central mooring, measuring temperature and salinity at depths of 30 cm and 6.5 m. Three autonomous profiling Seaglidors followed survey patterns of several tens of kilometers centered around the moorings, each collecting four to five profiles per day of temperature, salinity, and other variables from the surface to a depth of 1,000 m. Several other platforms contributed measurements, including special salinity surface drifters, mixed-layer Lagrangian floats, turbulence profilers, autonomous underwater vehicles (AUVs), and ships; these measurements are not discussed further here, but they provide other valuable data for understanding upper-ocean salinity in SPURS.

The surface buoy of the SPURS-1 central mooring was equipped with a full complement of meteorological instruments at a height of about 3 m above the sea surface to measure air temperature, humidity, winds, barometric pressure, precipitation, and downward solar

and infrared radiation. These measurements were used together with measurements of SSS and sea surface temperature (SST) to estimate the air-sea fluxes of heat, momentum, and freshwater using a bulk-flux algorithm (Fairall et al., 2003). The IMET (Improved METeorological) instruments used on the buoy and the Fairall et al. (2003) bulk-flux algorithm are believed to be accurate in the annual-average to within 8 W m^{-2} for net heat fluxes, to within 6 cm yr^{-1} for evaporation rate, and to within about 10% for precipitation (Colbo and Weller, 2009).

The central mooring also measured the ocean currents over the depth range of 3–300 m using four acoustic Doppler current profilers (ADCPs) and two single-point current meters. These velocity measurements can be used together with the horizontal gradients of salinity estimated from the other SPURS measurements to estimate the contribution of horizontal advection to the evolution of salinity at the central mooring.

To estimate the horizontal gradients of salinity and temperature, all of the salinity and temperature measurements from the

moorings, gliders, floats, and ship surveys were mapped onto a regular spatial grid by an objective mapping technique, assuming a Gaussian spatial autocorrelation function in the horizontal with decorrelation scales of 75 km. The 75 km decorrelation scale was chosen to provide a level of smoothing that yielded acceptably small mapping errors. To produce an estimate of the fields at a given time, all the data within a 14-day window were considered, and the influence of differing acquisition times for each data point was taken into account by increasing the assumed “error” associated with each data point (i.e., how closely the map is constrained to match the observation), depending on when it was measured relative to the map time. Maps were produced for each day of the yearlong field campaign, and maps separated by roughly 10 days can be considered independent. The space-time scales represented in an objective mapping are not simple to determine (being a function of assumed prior statistics of signal and noise, the actual statistics of the signal and noise, and the sampling in time and space), but we expect that the mapping effectively represents spatial variations on 50 km horizontal scales and temporal variations at 20-day periods. Horizontal temperature and salinity gradients were estimated from the mapped fields by fitting a plane to the mapped field over a $50 \text{ km} \times 50 \text{ km}$ region centered on the central mooring. Figure 1c shows an example of the resulting mapped field, along with an indication of the input data going into the mapping during the month-long period shown.

THE SALINITY FIELD AND CONDITIONS DURING SPURS-1

The SPURS-1 study region was centered where, on average, surface salinity is highest in the North Atlantic (e.g., Figure 1a). In September and October 2012, when R/V *Knorr* was in the SPURS-1 study region to deploy the autonomous platforms that would collect measurements over the coming year, Aquarius satellite fields indicated that the highest salinities were slightly to the north of the

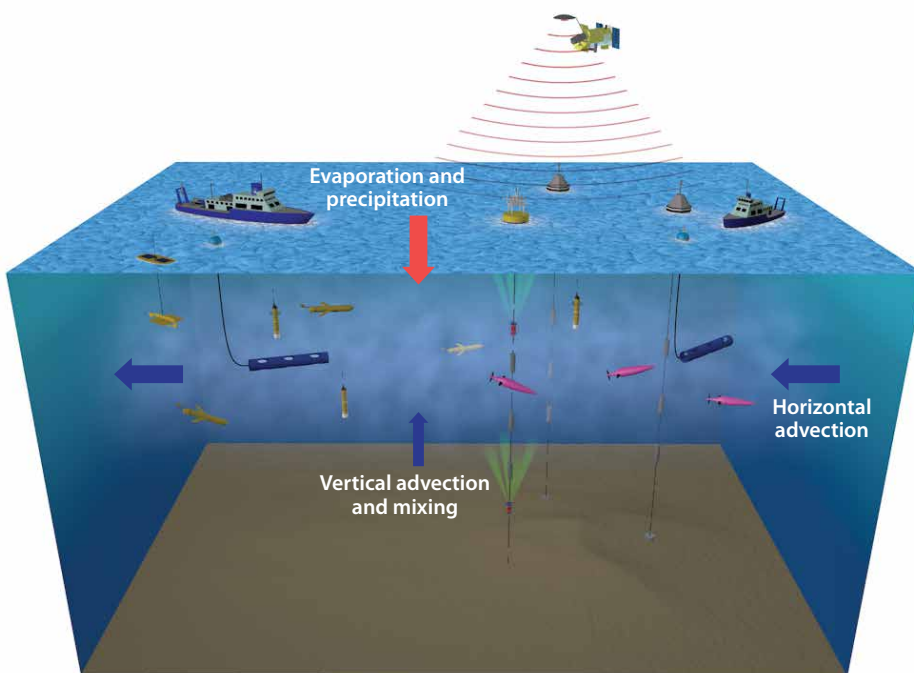


FIGURE 2. Depiction of the upper-ocean salt budget concept and the SPURS-1 measurement array. Evaporation and precipitation at the sea surface concentrate or dilute the saltwater and provide a “virtual salt flux” into the ocean. These surface fluxes, together with the net horizontal and vertical fluxes of salt by ocean currents and mixing processes, must be balanced by changes in ocean salinity. *Image credit: Jack Cook, Woods Hole Oceanographic Institution*

core of the SPURS array (Figure 1b). This northward surface salinity gradient is also clearly seen in the SPURS-1 data, with a mean increase in salinity of about 0.2 psu over the roughly 100 km from the southern to the northern part of the SPURS observational array during the month of October 2012 (Figure 1c). SPURS measurements also show variations on shorter temporal and spatial scales that have been averaged out in the analysis presented here. Some of these smaller-scale salinity variations are discussed by Shcherbina et al. (2015, in this issue), Riser et al. (2015, in this issue), and Hodges and Fratantoni (2014).

Temperature and salinity measured at the central mooring site over the one-year field program show a clear annual cycle, with a shallow, warm, and salty surface layer forming during the summertime (Figure 3). During fall and winter, this surface layer becomes fresher, cooler, and deeper, with most of this change occurring between November and February.

Qualitatively, the seasonal changes in upper-ocean salinity and temperature are consistent with the expected response to the seasonal cycle in the surface fluxes of freshwater, heat, and momentum. During the late spring and summer (April to September), there is relatively strong surface heating, along with steady evaporation and little rainfall (Figure 4). This would be expected to contribute to the formation of the shallow, warm, and salty mixed layers observed in the August to October periods of 2012 and 2013. Autumn and early winter (October to January) bring increased precipitation, stronger winds, and net surface heat loss to the atmosphere, conditions that would be expected to contribute to the deepening, freshening, and cooling of the mixed layer observed during that time.

SALINITY AND TEMPERATURE BALANCES IN SPURS DURING FALL AND WINTER

Coincident changes seen in upper-ocean temperature and salinity structures and in the surface fluxes of heat and freshwater

are suggestive of a direct link, but the SPURS-1 measurements allow us to distinguish between changes that occur in response to local surface fluxes and those driven by other processes, such as horizontal fluxes of different water masses. Here, we examine some of the terms in the salinity and temperature balances of the mixed layer, with a focus on the fall

and winter months (October to February) when the mixed layer was cooling, freshening, and deepening.

Using the temperature and salinity measured at the central mooring, we first identified the depth of the mixed layer, defined here as the depth where the potential density becomes 0.4 kg m^{-3} greater than the surface value (Figure 3).

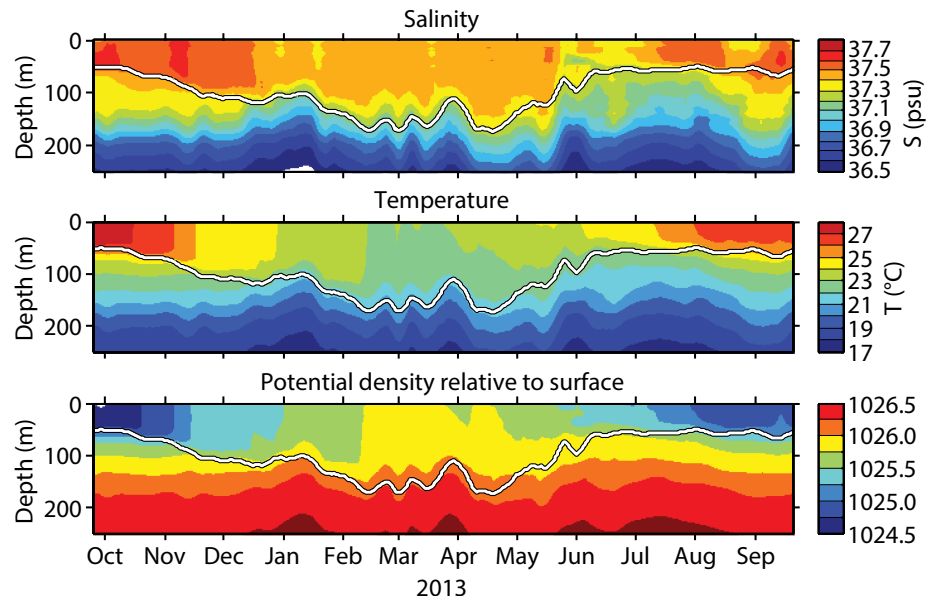


FIGURE 3. Depth-time evolution of salinity (upper panel), temperature (middle), and potential density relative to the surface (lower panel, in units of kg m^{-3}) at the central mooring site during the SPURS-1 campaign. (All data are shown as seven-day averages.) The thick white line indicates the base of the “surface layer” used for the salinity budget, defined as the depth where the potential density is 0.4 kg m^{-3} more than the surface value.

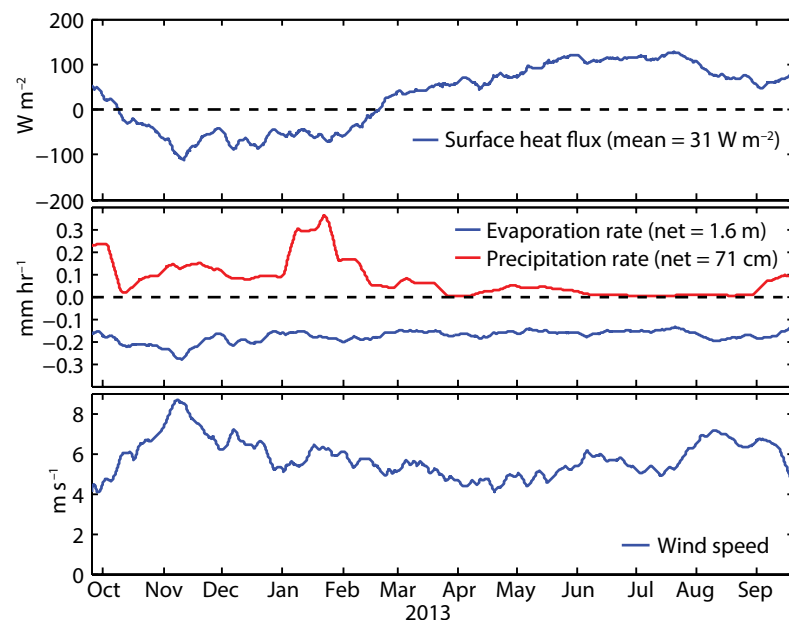


FIGURE 4. Evolution of surface heat flux (upper panel), evaporation and precipitation rates (middle panel), and wind speed (lower panel). All quantities have been smoothed over three weeks for display.

We averaged the salinity and temperature vertically over the layer and computed the rate of change using hourly averaged data. We estimated the horizontal advection terms (i.e., $\bar{u} \cdot \bar{\nabla S}$) using the layer-averaged velocities from the central mooring and the mapped salinity and temperature products described earlier. The mooring data allow a direct estimate of the surface flux terms ($(E-P)S/h$ and Q_o/h) using the surface heat and freshwater fluxes estimated from the buoy data (e.g., Figure 4). We used the data from the central mooring to make an explicit estimate of what we are calling the vertical entrainment term, $\hat{S}_{-h}(\partial h/\partial t)/h$, but we note that this is only a part of the group of terms that is more commonly referred to as the entrainment term (e.g., compare to Foltz et al., 2004).

For the turbulent salinity and heat fluxes at the base of the layer (i.e., F_{-h} and Q_{-h}), we follow the normal convention and model the turbulent flux as a “turbulent diffusion” that acts like molecular diffusion (but much more efficiently) to transport heat and salt vertically from high concentrations toward lower ones. Specifically, we take the turbulent salinity and heat fluxes at the depth h to be $F_{-h} = \kappa(\partial S/\partial z)$ and $Q_{-h} = \rho_c \kappa(\partial T/\partial z)$, where κ is the turbulent diffusivity. Centimeter-scale turbulence measurements from temperature microstructure probes on the Seagliders deployed during SPURS-1 suggest that the value of the turbulent diffusivity, κ , was between 10^{-7} and $10^{-5} \text{ m}^2 \text{ s}^{-1}$ at depth h during the time period considered here. Estimates from temperature and velocity microstructure collected during the September to October 2012 cruise using a more conventional microstructure profiler (the type used by St. Laurent, 2008) yielded cruise-averaged values of about $1\text{--}5 \times 10^{-6} \text{ m}^2 \text{ s}^{-1}$ at depths between 50 m and 800 m (Lou St. Laurent, Woods Hole Oceanographic Institution, *pers. comm.*, 2014). These preliminary estimates are lower than the more direct estimates by Ledwell et al. (1993) of turbulent diffusivity from a tracer release experiment at a nearby location (near 26°N, 29°W) at

about 300 m depth, which showed a time mean diffusivity of about $1.5 \times 10^{-5} \text{ m}^2 \text{ s}^{-1}$. For any of these values of κ , the turbulent flux terms will make only small contributions to the balance. The various SPURS-1 microstructure measurements will be analyzed and presented in detail elsewhere, and we only seek to bound the size of the turbulent flux terms here; we do so by using a large value for turbulent diffusivity at the depth h , $\kappa = 5 \times 10^{-5} \text{ m}^2 \text{ s}^{-1}$, and considering the range of likely values (error bounds) to be 10^{-7} to $10^{-4} \text{ m}^2 \text{ s}^{-1}$.

With the exception of the gradient terms from the mapped fields, all of the terms were estimated using hourly average data from the central mooring. The terms were then smoothed with a three-week running average to focus on the seasonal and intraseasonal evolution of salinity and temperature. The mapped fields can be considered statistically independent roughly every 10 days (see earlier discussion) and thus effectively resolve 20-day periods (commensurate with the 21-day smoothed fields from the mooring).

We made error estimates for all terms. For all of the terms except the subsurface turbulent flux (diffusion) terms, we estimated the errors using standard propagation of errors (e.g., Young, 1996, pp. 96–101) and reasonable assumptions about instrumental errors. A similar error estimate is presented in more detail in Farrar (2007, appendix to Chapter 3). We used the root-mean-square difference between the mapped temperatures and salinities and the measured ones as an estimate of the mapping error and used that value to estimate the error in the gradients determined from planar fits. We used estimates from Colbo and Weller (2009) for the errors in the surface fluxes. To bound the subsurface turbulent flux terms, we used a range of diffusivities (10^{-7} to $10^{-4} \text{ m}^2 \text{ s}^{-1}$) based on preliminary analyses of SPURS-1 turbulence measurements.

The sign of the rate of change of mixed-layer salinity ($\partial S/\partial t$) indicates whether salinity is increasing or decreasing with time. During the October to January

time period, it was negative on average (Figure 5), indicating a net decrease in salinity over the time period. Positive or negative values of the other terms indicate whether these terms tended to increase or decrease salinity. The surface flux term was typically positive because of the excess of evaporation over precipitation. The entrainment and turbulent flux terms were almost exclusively negative, indicating that these terms and the associated turbulent exchange with the fresher, deeper waters acted to decrease mixed-layer salinity. The turbulent flux (diffusion) term made relatively small contributions to the balance, even with our conservative assumption of a value of diffusivity that is larger than measurements suggest. The horizontal advection term was not systematically positive or negative, but instead had relatively large swings over time scales of one to two months.

The sum of the surface flux, turbulent flux, entrainment, and advection terms (black line in Figure 5) corresponds reasonably closely with $\partial S/\partial t$, and the sum of these terms can essentially explain the salinity changes observed over the time period to within the observational error. The overall balance is fairly complicated, with substantial contributions from all of the terms except the turbulent flux term. Although the correspondence of the seasonal cycle of the surface fluxes and the seasonal evolution of layer depth and salinity suggested a simple response to surface forcing, no one term can be said to be responsible for the freshening of the surface layer during the fall and winter months. However, it is clear that horizontal advection drove much of the salinity variability on time scales of one to two months during the time period examined here (compare red and green lines in Figure 5). For example, the correlation of the rate of change of mixed-layer salinity with the advection term ($R^2 = 0.53$) is higher than with any of the other terms. The combination of salinity gradients and currents that led to this advection-induced salinity variability is examined in the next section.

The mixed-layer temperature balance (Figure 6) is somewhat simpler, and there is a better match between the rate of change of mixed-layer temperature and the sum of the terms estimated. For example, the squared correlation coefficient between the rate-of-change term and the sum of the other terms is $R^2 = 0.71$ for the temperature balance versus $R^2 = 0.49$ for the salinity balance. The bulk of mixed-layer cooling happened during October and November 2012, when there were almost equal contributions from the surface flux, entrainment, and advection terms, as well as an appreciable contribution from the estimated turbulent flux term. Remarkably, the sum of these terms almost perfectly accounts for the observed $\partial T/\partial t$ during this time period. The mixed layer cooled at a slower rate during December and January, and the balance of terms was more variable then, too. The mixed-layer cooling ceased in January 2013, when horizontal advection brought in warm water to offset the cooling from the surface fluxes and entrainment terms. This advection event is analyzed in more detail in the next section.

DISCUSSION

We examined the balance of terms contributing to the evolution of mixed-layer salinity and temperature during fall and early winter of the SPURS-1 campaign near the location of climatological maximum sea surface salinity in the subtropical North Atlantic. We found that horizontal advection was an important term in the salinity and temperature balances on monthly time scales, but the budgets do not provide any direct insight into the complex physical processes responsible for this variability in the advection term and the resulting variability in the surface-layer salinity and temperature. Questions that arise include: Did the velocity vector rotate while the gradients remained steady? Vice versa? Did an eddy pass over the mooring at a particular time? To address these questions and provide an example of how evaluating the surface-layer salinity and temperature

balances can serve as a springboard for homing in on the physical processes influencing surface salinity and temperature, we decomposed the salinity and temperature advection terms ($\bar{u} \cdot \bar{\nabla} S$ and $\bar{i} \cdot \bar{\nabla} T$) to examine the individual components of the total advection term (Figures 7 and 8). The zonal and meridional currents (repeated in Figures 7b and 8b) and the zonal and meridional components of the gradients (Figures 7c and 8c) all exhibit variability and reversals during the four-month period considered here. There is no

obvious or simple relationship between the strength of the currents or the gradients and the magnitude of the total advection term. However, examination of the synoptic conditions at various times suggests that this month-to-month variability in advection results largely from the actions of mesoscale eddies. For example, in late January 2013, a time when the salinity and temperature advection terms were both large, examination of the dynamic sea surface topography field (using sea surface height anomalies from

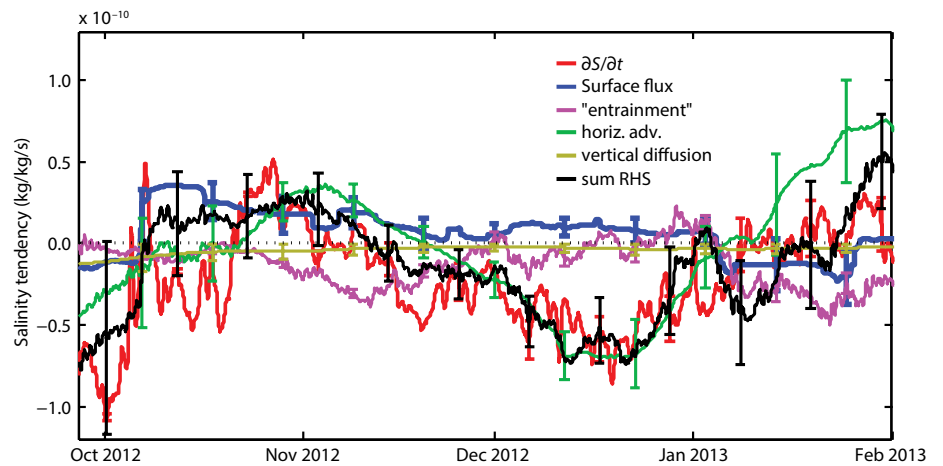


FIGURE 5. Terms in the mixed-layer salinity balance (Equation 2a) during the fall and winter months when the mixed layer was becoming fresher, cooler, and deeper. Positive values of (red line) indicate times when the measured mixed-layer salinity was increasing. Positive values of the other terms indicate that these terms are acting to make the mixed layer saltier. The vertical error bars indicate the expected errors for the various terms—the surface-layer salinity balance is typically closed within error bars (i.e., the red and black error bars overlap) during the fall/winter season.

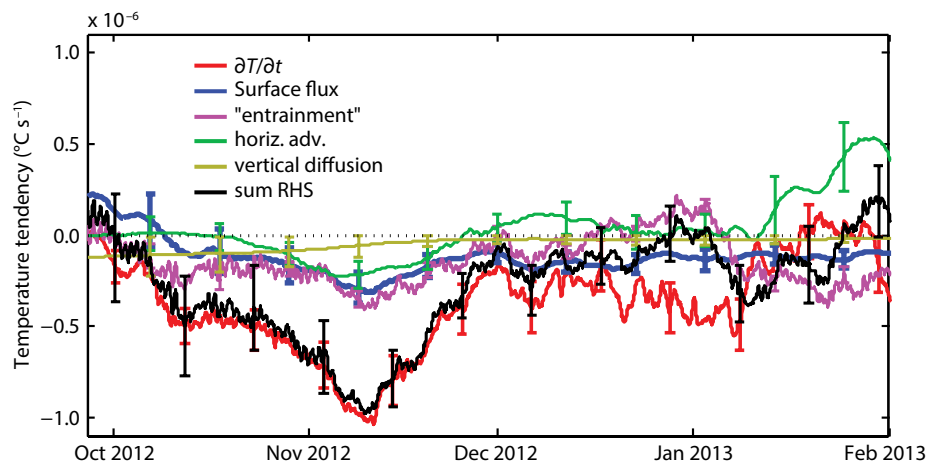


FIGURE 6. Terms in the mixed-layer temperature balance (Equation 3) during the fall and winter months when the mixed layer was becoming fresher, cooler, and deeper. Positive values of (red line) indicate times when the measured mixed-layer temperature was increasing. Positive values of the other terms indicate that these terms are acting to make the mixed layer warmer. The vertical error bars indicate the expected errors for the various terms—the surface-layer temperature balance is typically closed within error bars during the fall/winter season.

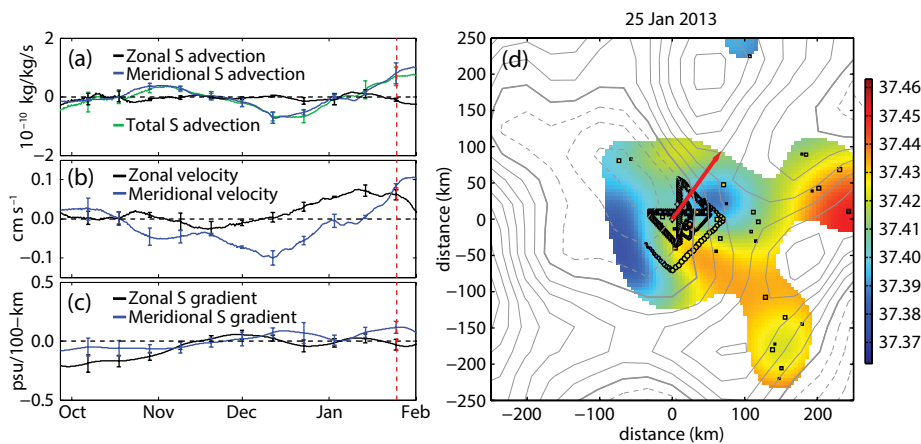


FIGURE 7. Decomposition of the salinity advection term in Equation 2a (left panels) and an example of the surface salinity field and geostrophic flow field during a time when advection of salinity was important (right panel). (a) Decomposition of the total advection term in Equation 2a (green line, repeated from Figure 5) into zonal (eastward; black) and meridional (northward; blue) advection. (b) Zonal and meridional components of layer-average horizontal velocity (21-day running averages). (c) Zonal and meridional components of the layer-average salinity gradient at the mooring site. The sign of these gradient components has been reversed for display so that the product of the blue lines (for example) in the lower two panels equals the blue line in the upper panel. (d) The mapped sea surface salinity field (colored) and sea surface dynamic topography (gray contours) on January 25, 2014, the time of large advection indicated by a vertical red line in panels (a)–(c). The 21-day averaged, layer-average velocity vector is shown in red, and the measurements used to estimate the surface salinity are indicated with symbols. The sea surface dynamic topography, or the dynamic contribution to sea surface height, is indicated with a 1 cm contour interval, using thin, solid lines for sea level highs and thin, dashed lines for sea level lows. The geostrophic flow will be counterclockwise around sea level lows. The increasing salinity in January 2013 is due to northward transport of high-salinity water on the south side of a counterclockwise-circulating mesoscale eddy.

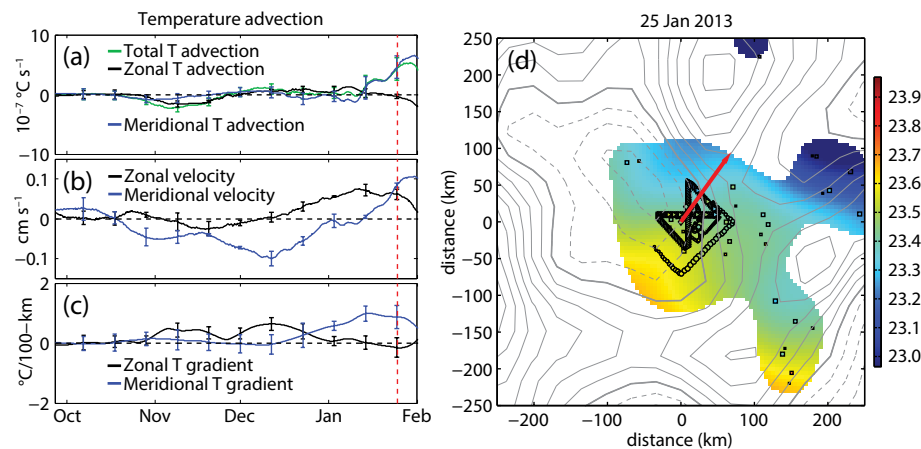



FIGURE 8. Decomposition of the temperature advection term in Equation 3 (left panels) and an example of the surface temperature field and geostrophic flow field during a time when advection of temperature was important (right panel; same time as in Figure 6). (a) Decomposition of the total advection term in Equation 3 (green line, repeated from Figure 5) into zonal (black) and meridional (blue) advection. (b) Zonal and meridional components of layer-average horizontal velocity (21-day running averages). (c) Zonal and meridional components of the layer-average temperature gradient at the mooring site. The sign of these gradient components has been reversed for display. (d) The mapped sea surface temperature field (colored) and sea surface dynamic topography (gray contours) for January 25, 2014, the time of large advection indicated by a vertical red line in panels (a)–(c). The 21-day averaged, layer-average velocity vector is shown in red, and the measurements used to estimate the surface salinity are indicated with symbols. The sea surface dynamic topography, or the dynamic contribution to sea surface height, is indicated with a 1 cm contour interval, using thin, solid lines for sea level highs and thin, dashed lines for sea level lows. The geostrophic flow will be counterclockwise around sea level lows. The increasing temperature in January 2013 can be seen to be due to northward transport of warm water on the south side of a counterclockwise-circulating mesoscale eddy.

the AVISO product described by Pascual et al. [2006] and the mean dynamic topography of Maximenko et al. [2009]) shows that the SPURS-1 central mooring was on the southeast side of a mesoscale eddy (Figures 7d and 8d).

The eddy’s counterclockwise geostrophic circulation around the sea level low brought warm and salty water from the southwest in late January (Figures 7 and 8). Despite this relatively large influx of warm, salty water to the mooring site by horizontal advection, the surface-layer temperature and salinity remained virtually unchanged (e.g., Figure 3). The salinity and temperature balances indicate that this was partly because of compensating contributions from surface heat loss and precipitation and from entrainment of cooler and fresher water from below the surface layer as it deepened.

We look forward to improving upon these preliminary salinity and heat budgets and using them to sharpen the focus on the ways that ocean dynamics and air-sea interaction affect the evolution of upper-ocean salinity. A rich variety of salinity measurements with high spatial resolution were made within the SPURS-1 array, and we expect to be able to make more direct estimates of some terms in the salt and heat budgets. In particular, we expect to be able to improve upon the advection estimate by making explicit estimates of terms that were left as residual terms here (Equation 2b), and to make more direct use of turbulence measurements made from several platforms during SPURS-1.

Evaluation of surface-layer budgets has been a common practice for gaining insight into the physical processes affecting the evolution of upper-ocean properties (e.g., McPhaden, 1982; Niiler and Stevenson, 1982; Foltz et al., 2004; Colbo and Weller, 2007; Cronin et al., 2013; Holte et al., 2014). While this is certainly a useful tool, it is also widely appreciated that the choice of control volume influences the outcome of the calculations. The control volumes represent integrations or averages of the conservation equations

over space, and the budget equations or terms are almost invariably also averaged over time. This temporal and spatial averaging filters the contributions to the salinity or temperature variability, and it can minimize the influence of some terms (e.g., if the lower boundary of the control volume, h , is made very large in Equation 2, the surface flux and turbulent mixing terms will become increasingly less important). To some extent, this filtering is the reason we examine control-volume budgets; it allows us to bypass terms that were not measured or are not of interest in a particular context (e.g., Niiler and Stevenson, 1982, provides a good example). The high density of salinity and temperature measurements in SPURS-1 allows us to make a credible estimate of the three-dimensional salinity and temperature gradients with less averaging than has been required in the past, raising the possibility of examining the balance of terms at different spatial and temporal scales, which is something we will pursue during the coming months of SPURS analysis. 

ACKNOWLEDGEMENTS. We are indebted to the large group of engineers, scientists, technicians, and ships' crews who contributed to the collection of the in situ and satellite data discussed here. We are grateful for comments on the manuscript from two anonymous reviewers and for constructive suggestions from guest editor Frank Bryan. J.T. Farrar, A.J. Plueddemann, J.B. Edson, and the deployment of the central mooring were supported by NASA grant NNX11AE84G. L. Rainville, C. Lee, C. Eriksen, and the Seaglider program were supported by NASA grant NNX11AE78G. R. Schmitt was supported by NSF grant OCE-1129646. B. Hodges and D. Fratantoni were supported by NASA grant NNX11AE82G. The Prowler moorings were funded by PMEL. The data analysis was also supported by NASA grant NNX14AH38G. The sea surface height product was produced by Ssalto/Duacs and distributed by AVISO, with support from CNES (<http://www.aviso.altimetry.fr>). The Aquarius data (v2.0) were obtained from the Physical Oceanography Distributed Active Archive Center (PO.DAAC) at the NASA Jet Propulsion Laboratory (<http://podaac.jpl.nasa.gov>). This is PMEL publication #4175.

REFERENCES

Beron-Vera, F.J., J. Ochoa, and P. Ripa. 1999. A note on boundary conditions for salt and freshwater balances. *Ocean Modelling* 1:111–118, [http://dx.doi.org/10.1016/S1463-5003\(00\)00003-2](http://dx.doi.org/10.1016/S1463-5003(00)00003-2).

Bouriès, B., R. Lumpkin, M.J. McPhaden, F. Hernandez, P. Nobre, E. Campos, L. Yu, S. Planton, A. Busalacchi, A.D. Moura, and others. 2008. The Pirata program: History, accomplishments, and future directions. *Bulletin of the American Meteorological Society* 89:1,111–1,125, <http://dx.doi.org/10.1175/2008BAMS2462.1>.

Colbo, K., and R.A. Weller. 2007. The variability and heat budget of the upper ocean under the Chile-Peru stratus. *Journal of Marine Research* 65:607–637, <http://dx.doi.org/10.1357/002224007783649510>.

Colbo, K., and R.A. Weller. 2009. Accuracy of the IMET sensor package in the subtropics. *Journal of Atmospheric and Oceanic Technology* 26:1,867–1,890, <http://dx.doi.org/10.1175/2009JTECHO6671>.

Cronin, M.F., N.A. Bond, J.T. Farrar, H. Ichikawa, S.R. Jayne, Y. Kawai, M. Konda, B. Qiu, L. Rainville, and H. Tomita. 2013. Formation and erosion of the seasonal thermocline in the Kuroshio Extension recirculation gyre. *Deep-Sea Research Part II* 85:62–74, <http://dx.doi.org/10.1016/j.dsr2.2012.07.018>.

Durack, P.J. 2015. Ocean salinity and the global water cycle. *Oceanography* 28(1):20–31, <http://dx.doi.org/10.5670/oceanog.2015.03>.

Durack, P.J., and S.E. Wijffels. 2010. Fifty-year trends in global ocean salinities and their relationship to broad-scale warming. *Journal of Climate* 23:4,342–4,362, <http://dx.doi.org/10.1175/2010JCLI3377.1>.

Durack, P.J., S.E. Wijffels, and R.J. Matear. 2012. Ocean salinities reveal strong global water cycle intensification during 1950 to 2000. *Science* 336:455–458, <http://dx.doi.org/10.1126/science.1212222>.

Fairall, C.F., E.F. Bradley, J.E. Hare, A.A. Grachev, and J.B. Edson. 2003. Bulk parameterization of air-sea fluxes: Updates and verification for the COARE algorithm. *Journal of Climate* 16:571–591, [http://dx.doi.org/10.1175/1520-0442\(2003\)016<0571:BP0ASF>2.0.CO;2](http://dx.doi.org/10.1175/1520-0442(2003)016<0571:BP0ASF>2.0.CO;2).

Farrar, J.T. 2007. Air-sea interaction at contrasting sites in the eastern tropical Pacific: Mesoscale variability and atmospheric convection at 10°N. PhD thesis, Massachusetts Institute of Technology and Woods Hole Oceanographic Institution, 166 pp.

Foltz, G.R., S.A. Grodsky, J.A. Carton, and M.J. McPhaden. 2004. Seasonal salt budget of the northwestern tropical Atlantic Ocean along 38°W. *Journal of Geophysical Research* 109, C03052, <http://dx.doi.org/10.1029/2003JC002111>.

Gill, A.E. 1982. *Atmosphere-Ocean Dynamics*. Academic Press, San Diego, CA, 662 pp.

Hodges, B.A., and D.M. Fratantoni. 2014. AUV observations of the diurnal surface layer in the North Atlantic Salinity Maximum. *Journal of Physical Oceanography* 44:1,595–1,604, <http://dx.doi.org/10.1175/JPO-D-13-0140.1>.

Holte, J., F. Straneo, J.T. Farrar, and R.A. Weller. 2014. Heat and salinity budgets at the Stratus mooring in the southeast Pacific. *Journal of Geophysical Research* 119:8,162–8,176, <http://dx.doi.org/10.1002/2014JC010256>.

Ledwell, J.R., A.J. Watson, and C.S. Law. 1993. Evidence for slow mixing across the pycnocline from an open-ocean tracer-release experiment. *Nature* 364:701–703, <http://dx.doi.org/10.1038/364701a0>.

Maximenko, N., P. Niiler, M.-H. Rio, O. Melnichenko, L. Centurioni, D. Chambers, V. Zlotnicki, and B. Galperin. 2009. Mean dynamic topography of the ocean derived from satellite and drifting buoy data using three different techniques. *Journal of Atmospheric and Oceanic Technology* 26:1,910–1,919, <http://dx.doi.org/10.1175/2009JTECHO672.1>.

McPhaden, M.J. 1982. Variability in the central equatorial Indian Ocean: Part II. Oceanic heat and turbulent energy balances. *Journal of Marine Research* 40:403–419.

Niiler, P.P., and J.W. Stevenson. 1982. The heat budget of tropical ocean warm water pools. *Journal of Marine Research* 40:465–480.

Pascual, A., Y. Faugère, G. Larnicol, and P.-Y. Le Traon. 2006. Improved description of the ocean mesoscale variability by combining four satellite altimeters. *Geophysical Research Letters* 33, L02611, <http://dx.doi.org/10.1029/2005GL024633>.

Qu, T., S. Gao, and I. Fukumori. 2013. Formation of salinity maximum water and its contribution to the overturning circulation in the North Atlantic as revealed by a global general circulation model. *Journal of Geophysical Research* 118:1,982–1,994, <http://dx.doi.org/10.1002/jgrc.20152>.

Riser, S.C., J. Anderson, A. Shcherbina, and E. D'Asaro. 2015. Variability in near-surface salinity from hours to decades in the eastern North Atlantic: The SPURS region. *Oceanography* 28(1):66–77, <http://dx.doi.org/10.5670/oceanog.2015.11>.

Schmitt, R.W. 2008. Salinity and the global water cycle. *Oceanography* 21(1):12–19, <http://dx.doi.org/10.5670/oceanog.2008.63>.

Schmitt, R.W., and A. Blair. 2015. A river of salt. *Oceanography* 28(1):40–45, <http://dx.doi.org/10.5670/oceanog.2015.04>.

Shcherbina, A.Y., E.A. D'Asaro, S.C. Riser, and W.S. Kessler. 2015. Variability and interleaving of upper-ocean water masses surrounding the North Atlantic salinity maximum. *Oceanography* 28(1):106–113, <http://dx.doi.org/10.5670/oceanog.2015.12>.

St. Laurent, L. 2008. Turbulent dissipation on the margins of the South China Sea. *Geophysical Research Letters* 35, L23615, <http://dx.doi.org/10.1029/2008GL035520>.

Young, H.D. 1996. *Statistical Treatment of Experimental Data: An Introduction to Statistical Methods*. Waveland Press, Prospect Heights, IL.

AUTHORS. **J. Thomas Farrar** (jfarrar@whoi.edu) is Associate Scientist, Woods Hole Oceanographic Institution, Woods Hole, MA, USA. **Luc Rainville** is Principal Oceanographer, Applied Physics Laboratory, University of Washington, Seattle, WA, USA. **Albert J. Plueddemann** is Department Chair, Physical Oceanography, Woods Hole Oceanographic Institution, Woods Hole, MA, USA. **William S. Kessler** is Oceanographer, National Oceanic and Atmospheric Administration Pacific Marine Environmental Laboratory, Seattle, WA, USA. **Craig Lee** is Senior Principal Oceanographer, Applied Physics Laboratory, University of Washington, Seattle, WA, USA. **Benjamin A. Hodges** is Postdoctoral Scholar, Woods Hole Oceanographic Institution, Woods Hole, MA, USA. **Raymond W. Schmitt** is Senior Scientist, Woods Hole Oceanographic Institution, Woods Hole, MA, USA. **James B. Edson** is Associate Professor, University of Connecticut Department of Marine Sciences, Groton, CT, USA. **Stephen C. Riser** is Professor, University of Washington, Seattle, WA, USA. **Charles C. Eriksen** is Professor, University of Washington, Seattle, WA, USA. **David M. Fratantoni** is Chief Technology Officer, Horizon Marine Inc., Marion, MA, USA.

ARTICLE CITATION

Farrar, J.T., L. Rainville, A.J. Plueddemann, W.S. Kessler, C. Lee, B.A. Hodges, R.W. Schmitt, J.B. Edson, S.C. Riser, C.C. Eriksen, and D.M. Fratantoni. 2015. Salinity and temperature balances at the SPURS central mooring during fall and winter. *Oceanography* 28(1):56–65, <http://dx.doi.org/10.5670/oceanog.2015.06>.